Characterization of Custom-Designed Charge-Coupled Devices for Applications to Gas and Aerosol Monitoring Sensorcraft Instrument

Tamer F. Refaat[1], M. Nurul Abedin[2], Glenn R. Farnsworth[2],
Christopher S. Garcia[3], Joseph M. Zawodny[2]

[1]Science and Technology Corporation, Hampton, VA 23666
[2]NASA Langley Research Center, MS 468, Hampton, VA 23681
[3]Old Dominion University, Norfolk, VA 23652

ABSTRACT

Custom-designed charge-coupled devices (CCD) for Gas and Aerosols Monitoring Sensorcraft instrument were developed. These custom-designed CCD devices are linear arrays with pixel format of 512x1 elements and pixel size of 10x200 μm^2. These devices were characterized at NASA Langley Research Center to achieve a full well capacity as high as 6,000,000 e^-. This met the aircraft flight mission requirements in terms of signal-to-noise performance and maximum dynamic range. Characterization and analysis of the electrical and optical properties of the CCDs were carried out at room temperature. This includes measurements of photon transfer curves, gain coefficient histograms, read noise, and spectral response. Test results obtained on these devices successfully demonstrated the objectives of the aircraft flight mission. In this paper, we describe the characterization results and also discuss their applications to future mission.

Keywords: Charge Coupled Devices, Photon Transfer Characteristics, CCD Quantum efficiency

1. INTRODUCTION

The Gas and Aerosol Monitoring Sensorcraft (GAMS) is a passive remote sensing grating spectrometer that relies on the solar occultation technique[1]. Developed at NASA Langley Research Center (LaRC), GAMS is a compact size version of the Stratospheric Aerosol and Gas Experiment (SAGE) instrument. The instrument was designed to measure the vertical distribution of ozone, water vapor, aerosols, temperature and pressure in the mid-troposphere to the stratosphere, while reducing the mission cost by a factor of ten, compared to SAGE III remote sensing instrument[2, 3]. Beside reduced weight, size and power consumption and incorporating the idea of on-board processing, cost reduction was achieved by adopting the solar occultation passive remote sensing technique[1,2]. Avoiding expensive excitation sources, as in active remote sensors, solar occultation depends on the Sun as the radiation source. The variation of the absorption of the Sun radiation through the atmosphere is calibrated to measure the atmospheric species[4]. As the radiation spectrum is analyzed using a grating spectrometer, it is measured using a charge couple device (CCD) linear array[5, 6]. The main requirement for the GAMS CCD was a wide dynamic range, through large full well capacity, to increase the instrument sensitivity. Therefore, The GAMS CCDs were custom designed and manufactured by Loral Fairchild Imaging Sensors for this particular application. The goal was to achieve CCD devices with high sensitivity, large full well capacity while maintaining good linearity. In this paper, some of the characterization experiments of the GAMS CCDs are presented. The experiments were carried out at NASA LaRC and included the photon transfer and the spectral response characteristics. The photon transfer characteristics were used to obtain the device conversion factor (**K** in e^-/DN), and to define the read noise and the full-well capacity, while the spectral response characteristics were used to obtain the quantum efficiency. The experimental procedures and results are analyzed and discussed.

2. CCD INSTRUMENTATION LAYOUT

The GAMS CCDs were packaged in a 28-pin Kovar tub as shown in figure 1(a). A thermistor was installed in the package for temperature feedback. The CCD has a linear format with 536 total number of pixels, which include 512 active pixels and 12 dead pixels on each side. The dead pixels act as dark or background datum that exist in all measurements, as indicated in the sample output in figure 1(b), to reduce the uncertainties in the measured signal. The pixel size is 10x200 μm^2 with no dead space between them.

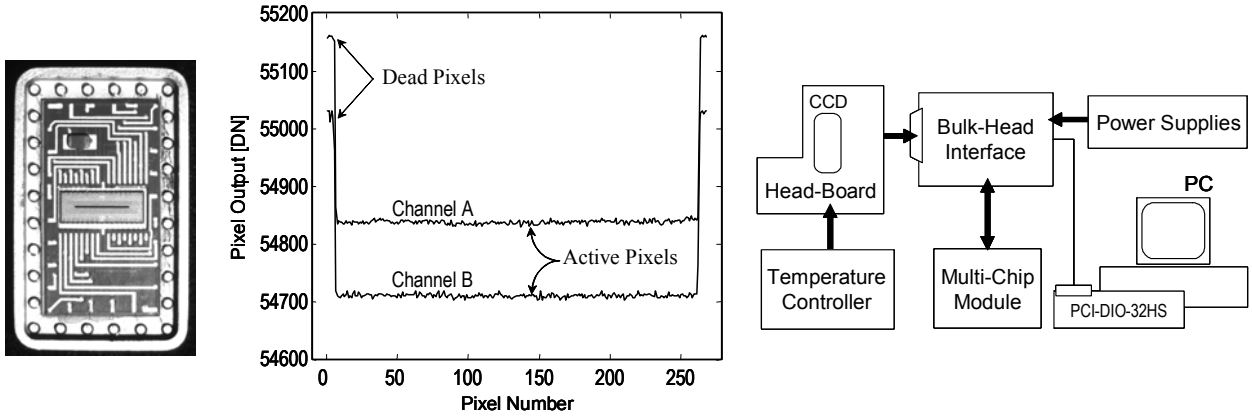

(a) (b) (c)

Figure 1 (a) 28-pin packaged CCD device. (b) The output signal for both channels, indicating active and dead pixels. (c) The read-out and interfacing circuitry used to operate the device.

For read out purpose, the pixels are interleaved into two channels with two independent read-out electronic circuitry (namely Channel A and Channel B as indicated in figure 1(b)). A schematic of the read-out and interfacing electronics, designed and fabricated at NASA LaRC, is shown in figure 1(c). The read-out and interfacing electronics are similar to the actual circuitry used in the GAMS instrument. The circuitry mainly includes a head-board, bulk-head interface, multi-chip module, power supplies and a personal computer along with a data acquisition card (National Instruments; PCI-DIO-32HS). The CCD is mounted directly to the head-board which contains signal conditioning electronics and analog-to-digital (ADC) converters (16 Bit, 100 kSPS) for channels A and B outputs. Besides, the head-board transmits the input clocking and bias voltages to the CCD. The bulk-head interface acts mainly as buffering stage for the digital output coming from the CCD through the ADCs to the personal computer. Also the same circuit provides the necessary driver electronics to the clock circuit and offset voltage reference applied to the device. With a base clock of 16 MHz, the multi-chip module provides all the necessary timing and clocking schemes to the CCD, and rearrange these schemes to match a specific integration time set by the user. After digital conversion and buffering, the CCD output is applied to the data acquisition card that collects the data and stores it in the personal computer. A user interface program allows external setting for several operating parameters such as the integration time and the averaging if required. The head-board design allows access to the bottom of the CCD package in order to attach a thermoelectric cooler (TEC) to set the tub temperature, along with the device, using an external temperature controller. The power supply, from Far West Sensors, provides the necessary power for the electronic circuits operation.

3. EXPERIMENTAL SETUP AND PROCEDURE

Several experiments were carried out for characterizing the GAMS CCDs. The operating conditions of each experiment was varied to obtain a specific characteristics. This includes varying the radiation intensity and the integration time for the photon transfer characteristics and varying the wavelength of the incident radiation for the spectral response characteristics. A characterization setup was integrated to perform these measurements, which consists of an optical and electrical sections. For a given operating condition, the optical section is used to apply a uniform radiation onto the device, while the electrical section is used to acquire the device output and store it into the computer for analysis.

3.1 Characterization Setup

The characterization setup is shown in figure 2. In the optical section, a current controlled tungsten halogen lamp is used as the radiation source, the output of which is spectrally analyzed using a monochromator. The monochromator inlet and outlet slits are set to 2.5 mm, resulting in a 20 nm resolution with 600 lines/mm grating. High pass filters were selected to block the higher order dispersion of longer wavelengths. A set of calibrated neutral density filters (NDF), installed on a double filter wheel, are used to control the intensity of the radiation in 0.1 dB steps. The filter wheel is followed by a diffuser to insure radiation uniformity. The CCD head-board is mounted on a three dimensional translation stage for alignment.

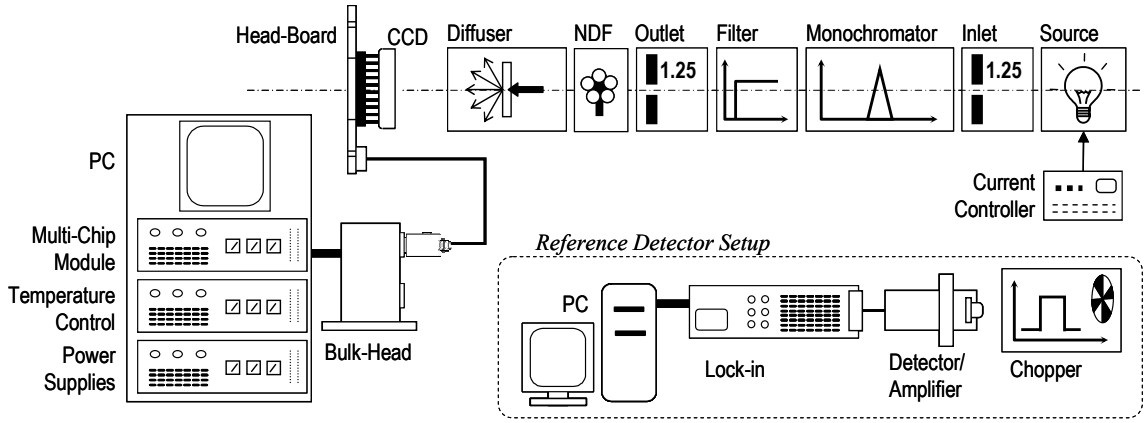

Figure 2. CCD characterization setup including both the optical and electrical sections. The inset shows the reference detector setup.

The electrical section mainly consists of the electronic circuitry discussed in section 2 (shown in figure 1(c)). A temperature controller was used to fix the device temperature. A 1x1 cm^2 diameter calibrated Si reference detector (Optronic Laboratories; OL 750-HSD-300) was used to measure the incident intensity for the CCD spectral response measurement, as indicated in the inset of figure 2. For the reference detector, an optical chopper was added to the setup for modulating the input radiation. Due to the different nature of the reference detector (single element versus linear array CCD) a separate electrical setup was used for the read-out. This setup consists of a pre-amplifier, for current to voltage conversion, the output of which is measured using a lock-in amplifier that is controlled and read by a second personal computer.

3.2 Theoretical Implementation and Procedure

For a specific operating conditions, in terms of device integration time and temperature and radiation intensity and wavelength, the data were collected from all the CCD pixels in the form of 400 successive shots, with no average. Therefore, assuming a certain characteristics, each data file corresponds to a single point in that characteristics. The data file in array format is generally represented by

$$\begin{array}{c} \\ \textbf{Pixels}\downarrow \end{array} \begin{array}{c} \textbf{Shots}\rightarrow \\ \begin{bmatrix} S_1^1 & S_1^2 & \cdots & S_1^{a-1} & S_1^a \\ S_2^1 & S_2^2 & \cdots & S_2^{a-1} & S_2^a \\ \vdots & \vdots & \ddots & & \vdots \\ S_{b-1}^1 & S_{b-1}^2 & & \ddots & \vdots \\ S_b^1 & S_b^2 & \cdots & \cdots & S_b^a \end{bmatrix} \end{array}, \tag{1}$$

where **a** is the total number of shots and **b** is the total number of pixels. Each element in the data file corresponds to an output digital number (DN) of the ADC. Therefore, S_n^m is an integer number between 0 and 65535 equal to the output of pixel **n** in shot **m**. The outputs of channel A and B are then separated using the pixel index **n**, where **n** is odd for channel A and even for channel B. The mean output signal from the active pixels, **S** (in DN), and its standard deviation or root-mean-square noise, **σ** (in DN), are then defined for every data point for each channel per shot, after subtracting the dead pixels reading according to the relations

$$S = \sum_{i=1}^{N_A} S_i \Big/ N_A - \sum_{j=1}^{N_D} S_j \Big/ N_D \text{ , and} \tag{2}$$

$$\sigma = \sqrt{\sum_{i=1}^{N_A} (S_i - S)^2 \Big/ N_A} \text{ ,} \tag{3}$$

where $\mathbf{N_A}$ and $\mathbf{N_D}$ are the number of the active and dead pixels per channel, respectively. For each data point, this process was repeated 400 times corresponding to the number of shots.

The characterization procedure starts by a spectral scan with the reference detector to measure the variation of the radiation intensity with wavelength, λ, while no NDF is used. Then, the test CCD is aligned to the same location of the reference detector, with respect to the radiation source, and the device output is recorded for the same intensity. The CCD responsivity, $\mathfrak{R}_{\mathbf{CCD}}$ (in A/W), is then calculated using the relation[7, 8]

$$\mathfrak{R}_{CCD}(\lambda) = \frac{\mathbf{q}\cdot\mathbf{K}}{\tau\cdot\mathbf{G}\cdot\mathbf{CF}}\cdot\frac{\mathbf{A}}{\mathbf{A_p}}\cdot\frac{\mathfrak{R}(\lambda)}{\mathbf{V_o}(\lambda)}\cdot\mathbf{S}(\lambda), \tag{4}$$

where $\mathbf{q}$ is the electron charge, $\mathbf{K}$ is the CCD conversion factor (in e^-/DN), τ is the integration time, $\mathbf{G}$ is preamplifier gain of the reference detector, $\mathbf{CF}$ is the lock-in amplifier correction factor, $\mathbf{A}$ is the reference detector area, $\mathbf{A_p}$ is the CCD pixel area (equal to the pixel size in this case), $\mathfrak{R}$ is the reference detector responsivity (in A/W), $\mathbf{V_o}$ is the reference detector output voltage and $\mathbf{S}$ is the CCD output signal per channel per shot, as obtained from equation (2). Then the quantum efficiency is achieved from the relation[7, 8]

$$\eta(\lambda) = \frac{\mathbf{h}\cdot\mathbf{c}}{\mathbf{q}\cdot\lambda}\cdot\mathfrak{R}_{CCD}(\lambda), \tag{5}$$

where $\mathbf{h}$ is the Plank's constant and $\mathbf{c}$ is the speed of light. It should be noted that the results of both equations (4) and (5) are dependent on the determination of the $\mathbf{K}$ value.

In order to obtain the $\mathbf{K}$ value of the CCD, a photon transfer curve was constructed[7, 9]. The photon transfer technique is one of the most powerful methods for calibrating the CCD system. Beside the $\mathbf{K}$ value, this technique is used to determine the read-noise and the full well capacity. The photon transfer curve is a relation between the noise and the average signal of a CCD. Generally, the CCD operation is associated with three main types of noise, namely the read noise, $\sigma_{\mathbf{R}}$, shot noise, $\sigma_{\mathbf{S}}$, and fixed pattern noise, $\sigma_{\mathbf{F}}$. The total CCD system noise is given by[10]

$$\sigma^2 = \sigma_R^2 + \sigma_S^2 + \sigma_F^2. \tag{6}$$

The read noise specifies the minimum noise related with the CCD operation. This noise is mainly due to all the associated electronics circuitry, therefore it is a constant and independent on the input signal. From dark to low signal level the read noise will be the dominant noise source. At higher signal level, the shot noise generated out of the random arrival of photons will be the dominant. From statistical aspect, the shot noise is given by[10]

$$\sigma_S = S^{1/2}. \tag{7}$$

Fixed pattern noise is generated due to slight asymmetry between the CCD pixels. This type of noise is the dominant at higher signal levels up to the saturation and is directly proportional to the signal. Considering the shot noise regime of the photon transfer curve, the $\mathbf{K}$ value can be obtained using the relation[7, 10]

$$\log(K) = \log(S) - 2\cdot\log(\sigma_S). \tag{8}$$

To obtain the photon transfer curve experimentally, the CCD was illuminated uniformly at a fixed wavelength with different intensity levels. The input intensity was varied using the NDF, starting with dark conditions, while keeping the current of the radiation source fixed. Signals obtained with this method were found adequate to determine the read-noise but insufficient to saturate the CCD and to define the full well capacity. For that purpose, the intensity was kept constant at its maximum and the CCD integration time was increased, while continually exposing the device (i.e. infinite exposure time). Practically, changing the integration time was easier than changing the exposure time to avoid source-device synchronization problems. For all the collected data, the signal and noise were calculated using equations (2) and (3) and then plotted in a logarithmic scale.

4. RESULTS AND DISCUSSION

Several CCD devices were characterized using the procedures discussed above. In this section the characterization results are presented in details for the two channels of one device (CCD 71). The results include the photon transfer curves, the modified photon transfer curves and the statistical evaluation of the **K** factor for both channels. A summary of the final results of all the characterized devices are tabulated. Finally, the spectral response and the quantum efficiency are given and discussed.

4.1. Photon Transfer Characteristics

The photon transfer curves were obtained by analyzing the variable intensity and variable integration time data. Figure 3 shows the photon transfer curves for both channels of CCD 71. The data was obtained by illuminating the device with 700 nm radiation. The intensity was varied starting with dark conditions at an integration time of 7.6 ms. Due to setup limitation, the maximum achievable radiation intensity was 1.4×10^{-6} W/cm^2. This intensity was enough to define the read-noise region and part of the shot noise region. Then the integration time was varied starting from 3.9 ms (to obtain some overlap points as indicated in the figure at the ½ region) up to about 90 ms. The device saturation was obtained at an integration time of 75 ms, after which a couple more points were obtained to confirm the full-well capacity.

The shot noise region of the photon transfer curve is of special interest for defining the **K** value. This is done by fitting a line with ½ slope in that region and observing its intersection with the $\log(\sigma_s)=1$ datum[7, 10]. With the CCDs under investigation, a problem arises due to the small number of data points that fit that line, as indicated in figure 3, probably due to the relatively high read noise associated with this system. Therefore, a data correction was applied to emphasize the shot noise region by eliminating the fixed-pattern noise. Pixel non-uniformity or fixed-pattern noise elimination was achieved by obtaining the modified (or classical) photon transfer curve as suggested by Janesick[10]. In this method three successive shots were analyzed simultaneously. The output signal **S** is taken as the mean of the three signals obtained using equation (2) for the individual shots. The noise, σ is determined by first differencing shots 1 and 2 then shots 2 and 3 and lastly shots 1 and 3 and generating three standard deviations using equation (3). These values are then averaged together and divided by $\sqrt{2}$ yielding the final noise[10]. Figure 4 shows the modified photon transfer curve after fixed pattern noise removal, where now the shot noise dominating the whole signal above the read noise level. According to equation (8) the **K** value is obtained. The first few data points with zero slope defines the read noise and the last points with a slope of ∞ defines the full well capacity, as indicated in the figure. It should be noted that the read-noise and the full well capacity are not affected by the fixed pattern noise elimination. This due to the fact that the full well capacity is dependent on the maximum number of electrons that the device can handle and its noise independent, while the read-noise is dominating the noise at low signal level, where the fixed pattern noise has negligible influence.

The determination of the **K** value using the photon transfer method is associated with high uncertainty. Therefore the curve was repeated 397 times (equal to the number of shots minus 3 for the fixed pattern noise elimination) leading to 397 different values of **K**. The **K** values with a slop which is closest to the ½ slope (within 1%) were only considered to construct histograms, as indicated in figure 5. A histogram indicates the number of occurrence of a certain **K** value within a certain tolerance (bin size). The histogram is then fitted to a Gaussian (natural) distribution function, the mean and standard deviation of which define the **K** value and its tolerance, as indicated in the figure. It should be mentioned that all of the bin size, number of data points and how close the line fitting to the ideal ½ slope are factors affecting both the **K** value and its tolerance. For the read noise and the full well capacity, the average values and the standard deviation are calculated directly, assuming uniform distribution and listed in Table I. The same table summarizes the results of the rest of the characterized CCDs. All the characterization results were obtained using the same head-board, except for CCD 3A. As an overall observation, the **K** value of these CCDs are higher than average, which match the high full well capacity requirement. The tolerance in calculating the **K** value is less than 10%, with 293.4 e^-/DN as a mean value. Also higher read noise is observed for channel B compared to A for all the devices. Finally, increasing the temperature has the tendency to increase the all of the **K** value, read noise and the full well capacity.

4.2. Spectral Response and Quantum Efficiency

The spectral response of the CCD was measured applying the substitution method, in which the Si calibrated reference detector was used to measure the radiation intensity of the CCD optical signal. The reference detector output was

obtained with a 167 Hz chopping frequency in the 400 to 1100 nm wavelength range with 20 nm step. After aligning the CCD to the same location the output was recorded at the same wavelength steps. The integration time was fixed at 7.6 ms with the NDF open and the CCD temperature was fixed at 19°C. Figure 6 shows the CCD spectral response and the quantum efficiency for both channels and the corresponding curve fitting. Peak responsivity of 0.28 and 0.29 A/W, for channels A and B respectively, was observed around 740 nm, corresponding to the Si energy bandgap. The quantum efficiency has an almost flat response in the 450 to 700 nm which matches the theoretical performance of a backside illuminated device. The quantum efficiency starts to roll-off at longer wavelengths due to the insufficient radiation energy. At shorter wavelengths, the quantum efficiency is limited by surface recombination effects.

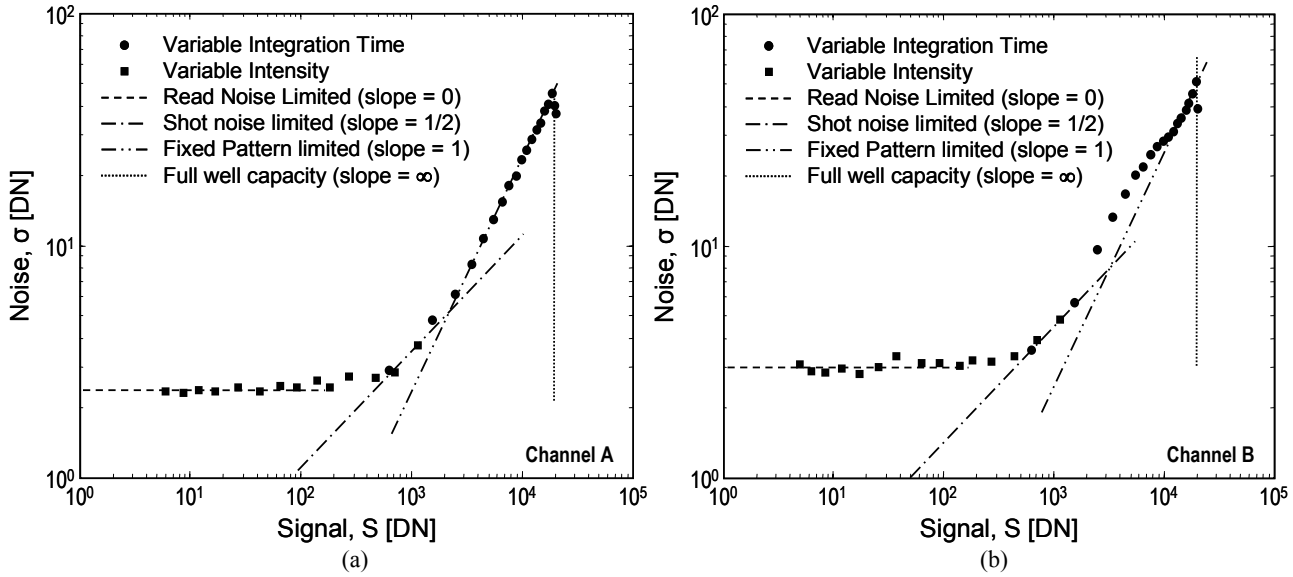

Figure 3. Photon transfer characteristics sample for the two channels of the characterized CCD 71 at 19°C. The curves obtained using variable intensity and variable integration time. The curves show different slopes corresponding to different dominating noise type.

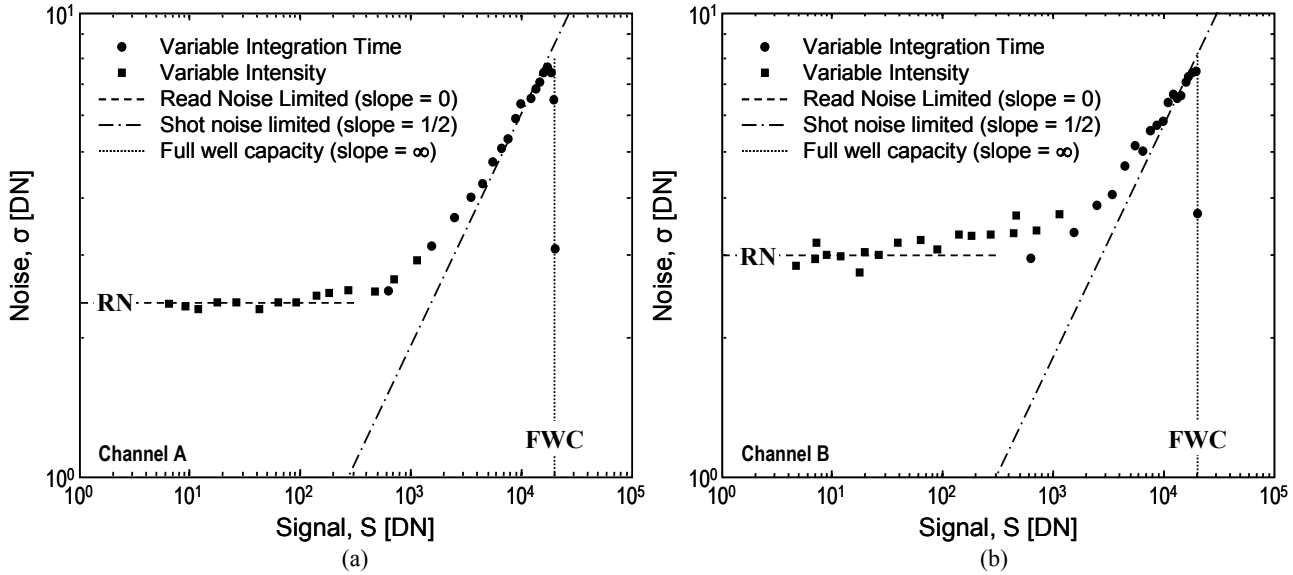

Figure 4. Modified photon transfer characteristics after eliminating the fixed pattern noise for the CCD 71 sample at 19°C. The curves define the **K** value, the read noise (RN) and the full well capacity (FWC) for this sample shot for both channels.

Table I Summary of the CCDs characterization results.

CCD	T (°C)	K (e^-/DN)		Read-Noise (e^-)		Full Well Capacity (e^-)	
		Ch A	Ch B	Ch A	Ch B	Ch A	Ch B
3A	19	296.8±25.9	297.5±23.3	755.9	762.5	4366818.4	4425312.5
3A	35	309.0±26.2	310.9±24.1	824.0	831.0	4614606.0	4689304.7
6A	19	309.1±31.5	285.5±30.7	726.4	790.8	4669264.6	4384138.0
7A	19	309.2±29.8	293.9±22.6	727.1	818.4	4479689.6	4306516.7
27	19	291.9±23.0	300.8±20.8	678.7	848.6	4392219.3	4144121.6
71	19	271.8±21.2	280.7±16.9	627.9	811.3	5421322.8	5600245.7
71	26	272.1±16.6	278.3±17.0	646.2	811.6	5467849.5	5601900.7

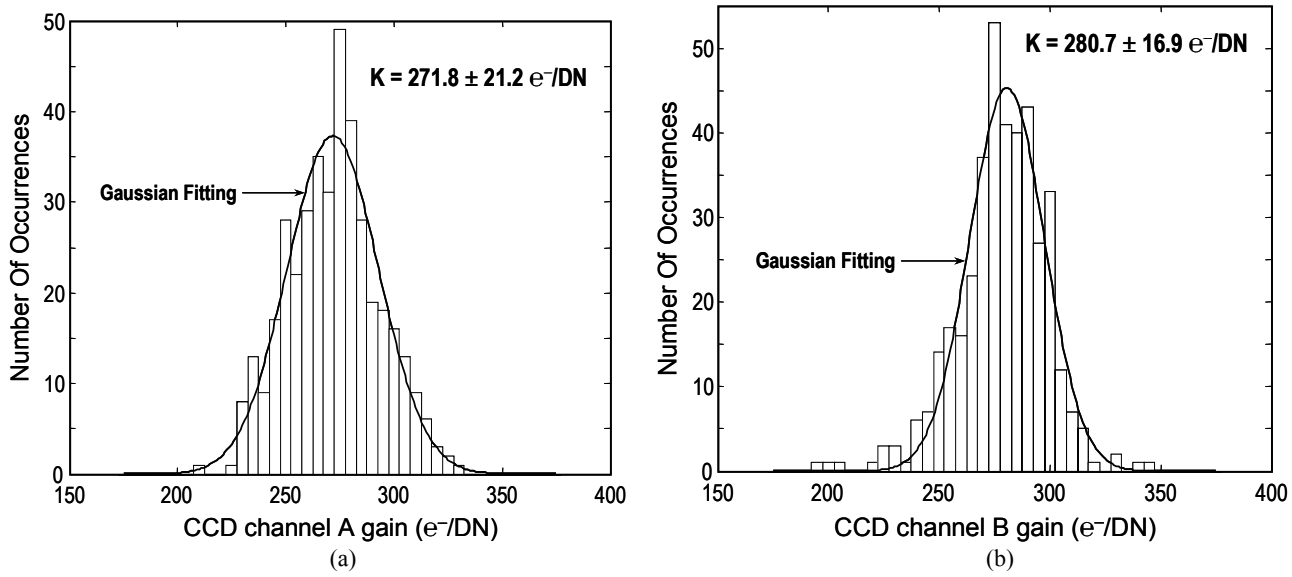

(a) (b)

Figure 5. Histogram plots for the **K** value for CCD 71 at 19°C, obtained with 5 e^-/DN bin size and the Gaussian distribution fit. The curves also shows the mean and the standard deviation of the fit for both channels.

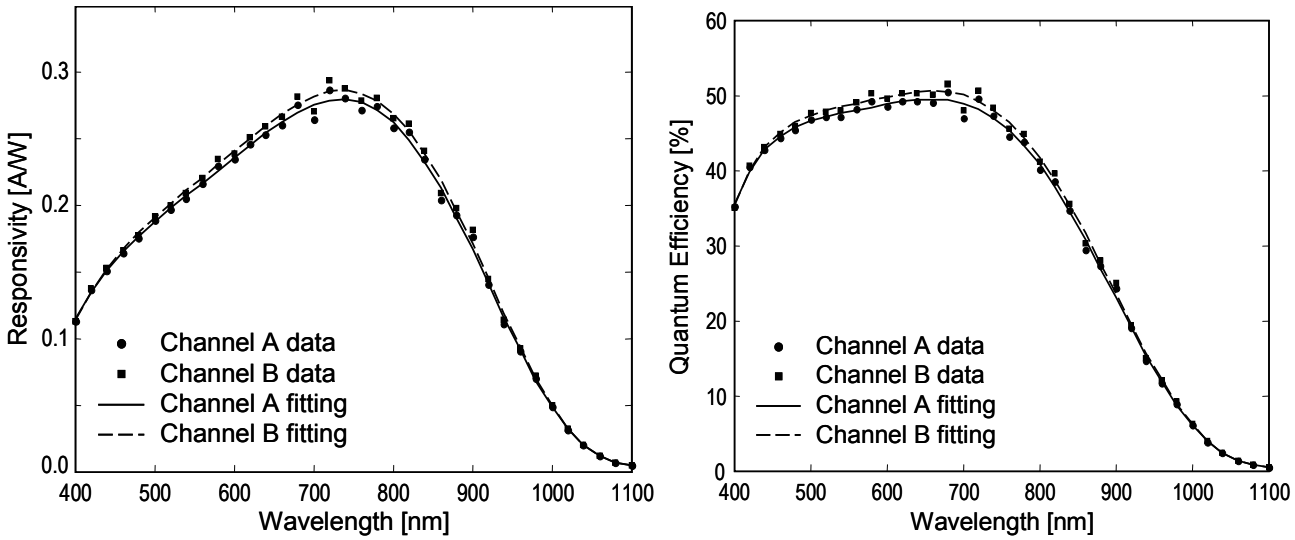

(a) (b)

Figure 6 Spectral response (a) and quantum efficiency (b) of channel A and channel B for CCD 71 obtained at 19°C and the corresponding curve fit.

Table II Fitting parameters for the responsivity and quantum efficiency curves shown in figure 6 for CCD 71 at 19°C. The parameters are valid in the wavelength range 400 to 1100 nm.

$f(\lambda) =$	$\Re_A$ (A/W)	$\Re_B$ (A/W)	η_A (%)	η_B (%)
p_0	5.9921	5.8753	-2.0563×10^{3}	-2.2286×10^{3}
p_1	-8.691×10^{-2}	-8.6882×10^{-2}	1.6784×10^{1}	1.8278×10^{1}
p_2	4.8956×10^{-4}	4.9422×10^{-4}	5.2210×10^{-2}	-5.7573×10^{-2}
p_3	-1.4215×10^{-6}	-1.4431×10^{-6}	7.5506×10^{-5}	8.5781×10^{-5}
p_4	2.3429×10^{-9}	2.3871×10^{-9}	-3.9256×10^{-8}	-5.0470×10^{-8}
p_5	-2.2068×10^{-12}	-2.2535×10^{-12}	-2.0199×10^{-11}	-1.3331×10^{-11}
p_6	1.1035×10^{-15}	1.1286×10^{-15}	3.1047×10^{-14}	2.8915×10^{-14}
p_7	-2.2683×10^{-19}	-2.3223×10^{-19}	-9.6094×10^{-18}	-9.3640×10^{-18}

Generally, both the responsivity and quantum efficiency could be fitted against the wavelength using polynomial equation in the form of

$$f(\lambda) = \sum_{x=1}^{X} p_x \cdot \lambda^x \tag{9}$$

where p_x is the fitting parameter for the power **x**. Table II list the fitting parameters for the responsivity, $\Re_A$ and $\Re_B$, and quantum efficiency, η_A and η_B, for channels A and B respectively, as indicated in figure 6.

5. SUMMARY AND CONCLUSION

In this paper the characterization results of a custom-designed Si based CCDs were presented. The characterized CCDs were custom designed for the GAMS instrument with large full well capacity. The **K** factor showed a higher values compared to regular CCDs. This is due to the special design of these devices to increase the system gain and sensitivity. These devices exhibit a wider full well capacity to increase the detection range. The mean **K** value obtained was 293.4 e^-/DN with less than 10% tolerance. The mean values of the read noise and the full well capacity are 761.5 e^- and 4754522.2 e^-, respectively, with tendency to be increased at higher temperatures. Spectral response and quantum efficiency measurements were presented for CCD 71 at 19°C and indicated a close match between both channels. These CCDs will be space qualified and could be useful for future airborne, spaceborne and planetary remote sensing missions.

REFERENCES

1. M. Koch, S. Sandford and J. Zawodny, "Next generation remote sensing: Gas and aerosol monitoring sensorcraft", Multispectral Imaging for Terrestrial Applications II, SPIE Proceedings, Vol. 3119, 80-89, 1997.
2. M. Grant and S. Sandford, "Real-time digital signal processing enables a reduced-cost atmospheric remote sensorcraft", Proceedings of the 17th Digital Avionics System Conference, Vol. 1, 1-8, 1998.
3. G. Halama, J. McAdoo, M. Jhabvala, A. Ewin, M. Fortin, R. Bredthauer, N. Abedin, "SAGE III alternative detector design and characterization", Proceeding of SPIE, Vol. 3756, 172-189, 1999.
4. M. McCormick, "Measurement of tropospheric aerosols from space using solar occultation techniques", NASA Technical Memorandum, NASA TM-4331, page 234, 1992.
5. J. Janesick, T. Elliott, S. Collins, M. Blouke and J. Freeman, "Scientific charge-coupled devices", Optical Engineering, Vol. 26, No. 8, 692-714, 1987.
6. S. Hsieh and H. Hosack, "Low light level imaging with commercial charge-coupled devices", Optical Engineering, vol. 26, no 9, 884-889, 1987.
7. J. Janesick, "CCD transfer method - standard for absolute performance of CCDs and digital CCD camera systems", Proceeding of SPIE, Vol.3019, 70-120, 1997.
8. K. Marien and E. Pitz, "Measurement of the absolute quantum efficiency of a charge-coupled device in the ultraviolet", Optical Engineering, Vol. 26, no. 8, 742-746, 1987.
9. J. Janesick, K. Klaasen and T. Elliott, "Charge-coupled-device charge-collection efficiency and the photon-transfer technique", Optical Engineering, Vol. 26, no. 10, 972-980, 1987.
10. J. Janesick, *Scientific Charge-Coupled Devices*, Chapters 2 & 3, SPIE Press, Bellingham, Washington, 2001.